# Diagnosing angular (directional) spectra by Tikhonov regularization (ridge regression, tapered least squares) in numerical studies of wave scattering (wave-topography interaction)

May 19, 2018


## Abstract

Realistic numerical simulations of wave propagation (both surface and internal) involve complex patterns of interference that conceals energy transfers. The elementary wave components can be deduced from angular spectrum. Here, the energy distribution is found by solving an inverse model based on plane wave dynamics. The solution method is a least square minimization augmented with penalizing term (Tikhonov regularization). This aids stability in presence of noise and provides better spectral resolution for under-sampled signal. Further, applicability of the method for energy estimates is tested against analytical solution of wave scattering by bottom topography. In the first problem a periodic shallow gravity wave attacks a circular island. The inverse model correctly identifies energy lobes and their amplitude, hence, allowing to examine scattering amplitude in more complex environments. In the second test, a low mode internal wave reflects from a continental slope represented as step topography. Estimated bulk reflection coefficient compares excellent with the analytical solution. But in case of three dimensional topography the method as well provides information on spatial variation of point-wise coefficient due to inhomogeneity of the prescribed incident field. The results lend confidence in robustness of the inverse technique, hence, suggesting its applicability to field observations of the real ocean.


## 1 Introduction

The oceanic waves interfere and create obscure character [1] in currents and pressure. The staggered pattern makes difficult to answer the simplest questions about waves: from where are they coming and how strong they are. Hence, there will always be an uncertainty in estimate of energy transfers and budgets. In an example of a standing wave, no energy transfer is taken place, yet two waves are present but oppositely traveling. The problem of

[1] (change?)

diagnosing elementary components inevitably emerges in studies of wave-topography interaction. Energy is transfered into scattered wave field that undoubtedly has large number of components. This might produce spatially (horizontally) tight beams of energy transport. Such phenomena was observed in numerical simulations of tsunami waves (Tang et al. (2012)) and internal waves of tidal frequency (internal tides) (Simmons et al. (2004), Arbic et al. (2010)(?)) (and in observations (Zhao et al. (2016))). To present a method to deduce dynamics of a complex wave field such as aforementioned ones is a chief reason for this note (chapter, paper).

A straightforward method is to obtain spatial frequencies of elementary waves (Barber (1963)) by means of two dimensional Fourier transform. It further can be mapped onto a circle leading to angular spectra. In the field studies this approach was extensively used in relation to surface wave phenomena, e.g. propagation (W. H. Munk et al. (1963), reflection (Dickson et al. (1995), Thomson et al. (2005), island diffraction (Pawka (1983)). The spectral description was also applied to tsunami trapping (Romano et al. (2013)) and internal tide propagation (Hendry (1977), Lozovatsky et al. (2003)). Estimation of spectra is a problem that one encounters and here is dealt by inverse modeling (Long (1986)). As discrete Fourier transform leads to ambiguity in elementary wave direction, additional inferences are necessary. Even though application of the Hilbert transform can resolve the issue (Mercier et al. (2008)) [2], it does not utilize all wave field characteristics available. Logically, constrains of wave dynamics are expected to lessen Gibbs phenomena, increase directional resolution and provide a way to super-resolution (Kay & Marple (1981), Sacchi et al. (1998)) so essential (viable, relevant, crucial) for resolving short-crested waves.

The inverse approach has to comprise dynamical statements of the wave field. So that angular spectrum will be related to (translated into) observed pressure and currents simultaneously. But such postulated problem leads to overdetermined and ill-posed system of equations, naive least square solution is unstable in relation to small changes or errors in data. For example, errors in numerical simulations might arise due to numerical and physical friction (reference?) leading to nonuniform wave amplitudes over sampling window of the numerical ocean. Hence, regularization is generally necessary to stabilize and improve inverse estimate (W. Munk et al. (2009), Snieder & Trampert (1999)). In studies of wind wave spectra this is a well known approach when penalizing terms are added to cost functions. These terms can comprise constrains on spectrum shape and smoothness (Long & Hasselmann (1979), Herbers & Guza (1990)), spectrum sparseness (Hashimoto & Kobune (1989), Sacchi & Ulrych (1996)[3], or statistical properties (Benoit et al. (1997)). Unfortunately, the mentioned methods cannot be utilized in studies of wave-topography interaction. The scattered field is "phase-locked" with incident one and thence, phase must be retained in the model equations (e.g. Thomson et al. (2005)) leading to deterministic wave decomposition. This is in contrary to wind waves of open sea that are mainly stochastic.

The simplest regularization technique, nevertheless powerful one seeks an inverse esti-

[2](Will it work with many components? In presence of corrugated surfaces?)

[3]this is geophysics reference

mate of minimum variance. Initially developed by Tikhonov et al. (2013) for solution of Fredholm integral equations, Tikhonov regularization has a wide application starting from theoretical work in acoustics (Colton & Kirsch (1996)) and holography (Williams (2001)) to observational oceanography (W. Munk et al. (2009)) and geophysics (Snieder & Trampert (1999)) where it is named "tapered" or "damped" least squares. But it has never been used [4] to oceanic wave problems. In the first section the inverse model will be formulated in order to find angular spectrum of waves. The developed approach than (Section 3) is illustrated on simple synthetic experiments to show its performance characteristics. And in later sections (4 and 5) is applied to numerical experiments of wave scattering where comparison with the well-known analytical solution is taken place. In section 6 concluding remarks are made and drawbacks are outlined.
[5]

# 2 Regularization technique of obtaining angular spectrum

## 2.1 Mathematical preliminary

Let pressure or sea level in complicated seas to be described by angular spectrum[6],

$$p(\vec{r},t) = \int_0^{2\pi} d\theta_k S(\theta_k) e^{i\vec{k}(\theta_k)\cdot\vec{r}+\phi(\theta_k)-i\omega t} \tag{1}$$

Here each elementary (monochromatic) sine wave of wavenumber $k$ travels in direction $\theta$ with energy $S(\theta)^2 d\theta$ and temporal (spatial) lag of $\phi(\theta)$. Through out the note temporal dependence is omitted and complex notation is inferred. It is sought to estimate the angular spectrum $S(\theta)$ and phase distribution $\phi(\theta)$ from a finite set of observations. At first, this problem is reformulated in terms of Fourier coefficients (Benoit et al. (1997), Rafaely (2004)) by application of Jacobi-Anger expansion [7],

$$p(r,\theta) = e^{i\vec{k}(\theta)\cdot\vec{r}} = \sum_{m=-\infty}^{m=\infty} i^m J_m(kr) e^{im(\theta-\theta_k)} \tag{2}$$

shows that a field at point $(r,\theta)$ produced by plane wave can be expanded in series of Bessel functions and circular functions. Than its substitution into (1) and reorganization lead to

$$p(r,\theta) = \sum_{m=-\infty}^{m=\infty} \Big[ \int_0^{2\pi} d\theta_k S(\theta_k) e^{i\phi(\theta_k)} e^{-im\theta_k} \Big] i^m J_m(kr) e^{im\theta} \tag{3}$$

Term in brackets (square brackets) represent convolution integrals defining Fourier coefficients of order $m$, $A_m - iB_m$. Thence, series (3) state a model equation to find the unknown

[4] Dushaw used similar inverse
[5] Should I add plane-wave fit? "subtraction" method of Jody (and Zygmunt)?
[6] This is not spectrum per se, is term usage still possible?
[7] (should I cite anything?)

coefficients from the known, measured pressure field. Its spatial distribution can be sampled at a set of points $(r_i, \theta_i)$ and infinite series are truncated at order $N$ both leading to matrix formulation[8],

$$p_i = \sum_{m=-N}^{m=N} J_m(kr_i)e^{im(\theta+\pi/2)}(A_m - iB_m) \tag{4}$$

Real and imaginary parts constitute two separate problems allowing deterministic definition of the spectrum. Angular spectrum and phase distribution will be recomposed as usual by

$$S(\theta_k)e^{i\phi(\theta_k)} = \frac{1}{\pi}A_0 + \frac{2}{\pi}\big[\sum_{m=1}^{m=N} A_m \cos m\theta_k + iB_m \sin m\theta_k\big]$$

The same steps are repeated but with current velocities instead, starting from (1) transfer functions are inserted invoking plane wave dynamics,

$$\begin{Bmatrix} u(\vec{r},t) \\ v(\vec{r},t) \end{Bmatrix} = \int_0^{2\pi} d\theta_k \frac{k}{\rho_0(\omega^2 - f^2)} \begin{Bmatrix} \omega k \cos\theta_k + if \sin\theta_k \\ \omega k \sin\theta_k - if \cos\theta_k \end{Bmatrix} S(\theta_k)e^{i\vec{k}(\theta_k)\cdot\vec{r}+\phi(\theta_k)} \tag{5}$$

Than dependence of currents on wave bearing causes splitting of Fourier coefficients and asymmetry via Coriolis effect,

$$\begin{Bmatrix} u_i \\ v_i \end{Bmatrix} = \frac{1}{2}\sum_{m=-N}^{m=N} J_m(kr_i)e^{im(\theta+\pi/2)} \begin{Bmatrix} (\omega-f)A_{m+1} + (\omega+f)A_{m-1} - i[(\omega-f)B_{m+1} + (\omega+f)B_{m-1}] \\ (\omega-f)B_{m+1} - (\omega+f)B_{m-1} + i[(\omega-f)A_{m+1} - (\omega+f)A_{m-1}] \end{Bmatrix} \tag{6}$$

This results points out that to describe velocity field higher circular harmonics have to be employed. Physically, velocity field has higher spatial variability. This is well known idea since spatial differentiation acts as a high-wavenumber filter (e.g. Rhines (1977)). But in (6) additionally, the asymmetry is observed for clockwise and counterclockwise components.[9]

## 2.2 Inverse technique formulation

Inverse model sets its goal an estimation of angular spectrum from observed field characteristics. This relation is posed by (4) and (6) and formally expressed as,

$$y = Kx \tag{7}$$

where $y$ measured pressure and currents, $x$ - Fourier coefficients and $K$ - model coefficients. The statement does not need to be strictly satisfied as the model might not be fully correct such as in case of non-planar waves or presence of errors. Additionally, $K$ does not have to be a square matrix, e.g. it is possible to have less measurements than unknowns. Hence, there will be a residue and measure of solution's success should be imposed, such as in least-square minimization, $\min\{||Kx - y||_2^2\}$ - to find a solution with minimum residue in $L_2$-norm sense.

[8] should i drop infinite series here?

[9] This is bad, but discussion is necessary

And the least-squares solution will be found as Moore-Penrose inverse (Bennett (1992)). Generally, it will be unstable to small errors in data and produce physically inconsistent results (ill-posedness). Addition of regularization parameter is to solve the issue. As in Tikhonov regularization, an inverse solution should minimize the following cost function,

$$x_\alpha = \arg\min\{||Kx - y||_2^2 + \alpha||x||_2^2\} \tag{8}$$

The second term controls amount of solution's variance with a weight $\alpha$ called a regularization parameter. It can be shown that this parameter represents a low-pass filter over orthonormal vectors of $K^TK$ (Williams (2001)). This becomes clear as solution is explicitly expressed,

$$x_\alpha = (K^TK + \alpha I)^{-1}K^Ty \tag{9}$$

So that factor $\frac{\lambda_k^2}{\lambda_k^2+\alpha}$ ($\lambda_k$ - singular value) is introduced to damp small singular values. Unfortunately, this decreases solution and exerts dependence of $x_\alpha$ on the regularization parameter: for $\alpha = 0$ regular least-square estimate is obtained, while for large $\alpha$ minimizer is close to zero. Its choice cannot be made a priori and has to be data-driven. In field studies this is usually set by a signal-to-noise ratio (W. Munk et al. (2009)), since it has to scale noise variance to actual signal's strength. Many techniques exist (Williams (2001)), but there is no silver bullet approach and everything depends on problem of interest. Here straightforward method will be used that is called L-curve (Hansen & OLeary (1993)).
As mentioned, in Tikhonov regularization amount of allowed error is competing with solution's norm. The simplest idea is to find an optimal parameter balancing both factors. This is seen as rapid change in behavior of curve associating residue with solution's norm as regularization varies (Figure 1). The two extremes for $\alpha \to 0$ and $\alpha \to \infty$ are observed as straight vertical lines. A sharp corner connects two regions and a point with maximum curvature is proposed to be used as a regularization parameter.

## 2.3 Synthetic example to illustrate method

The so-described method is not different as a regular Discrete Fourier transform of finite time series. Here, the spectrum is found over data-points organized in circular antenna, only spatially finite region is known (Figure 2a). The solution will have a finite number of orders and this will result in Gibbs ringing (Figure 2c). The role of regularization is seen in oversmooothing of the spectra and decrease of spectral resolution. In case of perfect model penalized least squares will always worse than direct fit. But as some inconsistency appear in the data (modeled here as white noise with 1% variance of main signal) the least squares result in unphysical spectrum. On the other hand, white noise improves the penalized least squares solution.
It is apparent that maximum order is a crucial characteristic for resolution. From the expression (ref-to-spectrum reconstruction) it is seen that two wave will be separated in principle if $\delta\theta \leq \frac{\pi}{N_{max}}$ (Rafaely (2004)). In the inverse model formulation this directly depends to Bessel function. And since these coefficients depend order and $kd_{antenna}$ only later can increase resolving power of the method. But if velocities are used in conjunction with pressure observations the order can be increased at least by one as follows from the inverse model formulation (6) where there is a shift between Bessel function and coefficients. In the following

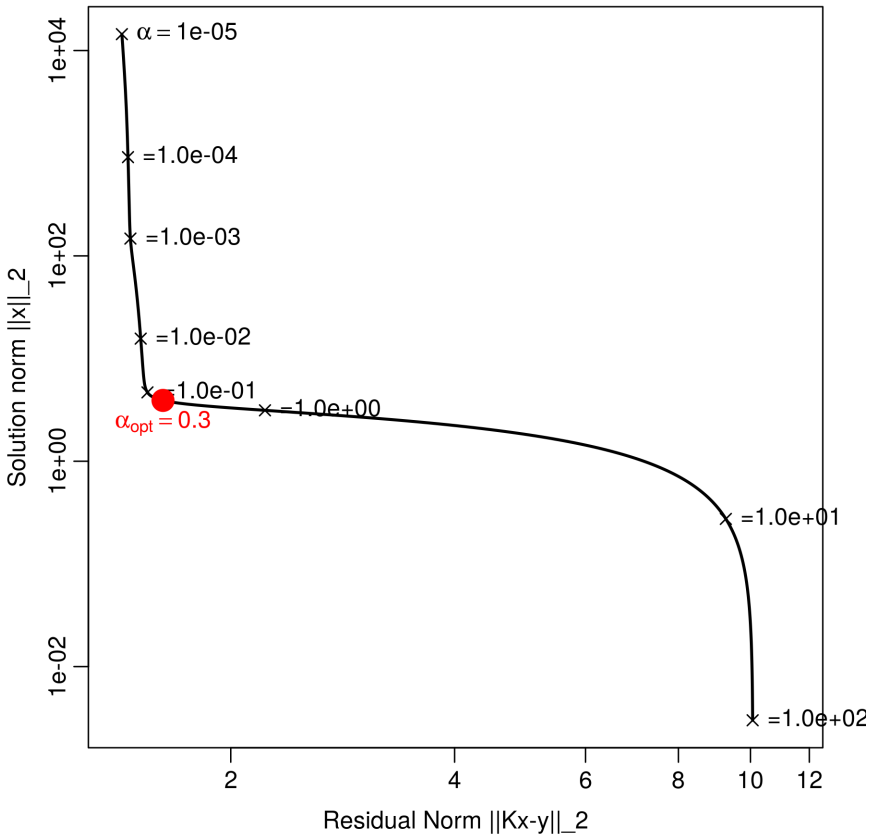


Figure 1: L-curve example

example two waves cannot be discerned since antenna size is two small to satisfy Rayleigh criteria, $sin\delta theta = 1.22\frac{\lambda}{d_{antenna}}$, so the reconstructed spectrum shows one smeared wave. But if velocities are augmented to the data, there is an increase in resolving power and waves are actually resolved.
Note in the numerical application observed velocities are scaled so that variance of residue will have similar magnitude with pressure.

Figure 2a: Antenna of data-points sampling a synthetic plane wave directed at 180°.
Figure 2b: Solution coefficients for the synthetic example: regular least squares, PLS, and with white noise added.
Figure 2c: Reconstructed spectrum of the wave field.

Figure 3a: Two wave interference with observational antenna not able to separate waves.
Figure 3b: Solution coefficients for inverse solution without and with velocity components used.
Figure 3c: Reconstructed spectrum of the wave field.

# 3 Test problems of wave scattering

The aim of this paper is to obtain spectrum which later is used to infer physical properties of wave-topography interaction. In the case of wave interaction there is an energy transfer from incident wave into scattered. And spectrum can be used to delineate this energy process. Usually, a researcher is interested in spatial characteristics of scattered wave field (cite Sato?) or in some bulk quantity such as reflection coefficient (Klymak et al. (2016)). These two problems will be studied by application of the proposed method. The simplest problem are taken for which analytical solution is well known, so that comparison between the method result and exact solution could be made. Additionally, auxiliary experiment is carried out with no topography which result is subtracted from the total field so that exact scattered wave in terms of numerical experiments can be studied.

## 3.1 Example diffraction of shallow-gravity wave

The infitinite periodic wave train is sent impinging on a seamount represented by a cylinder of radius 40 km rising from plane bottom ocean of depth 5km to the depth of 250 m. The 3 experiments of different period are performed. In the numerical experiment it is used the simplified numerical code developed by (Kowalik et al. (2005)). All nonlinear terms were neglected, while bottom friction is controlled by constant coefficient of $3.3 \cdot 10^{-3}$. The integration is carried out over grid with resolution of 2 $km$ by 2 $km$. The boundaries are open, so all scattered waves are traveled away without reflection. The periods are taken to be 10, 15 and 20 min so that different regimes in response can be caught such as Diffraction and No-interaction.
After quasi-equilibrium is reached temporal Fast Fourier transform is employed to find amplitude and phase of the strongest wave at each grid point (Figure 4a). Than Fourier coefficients

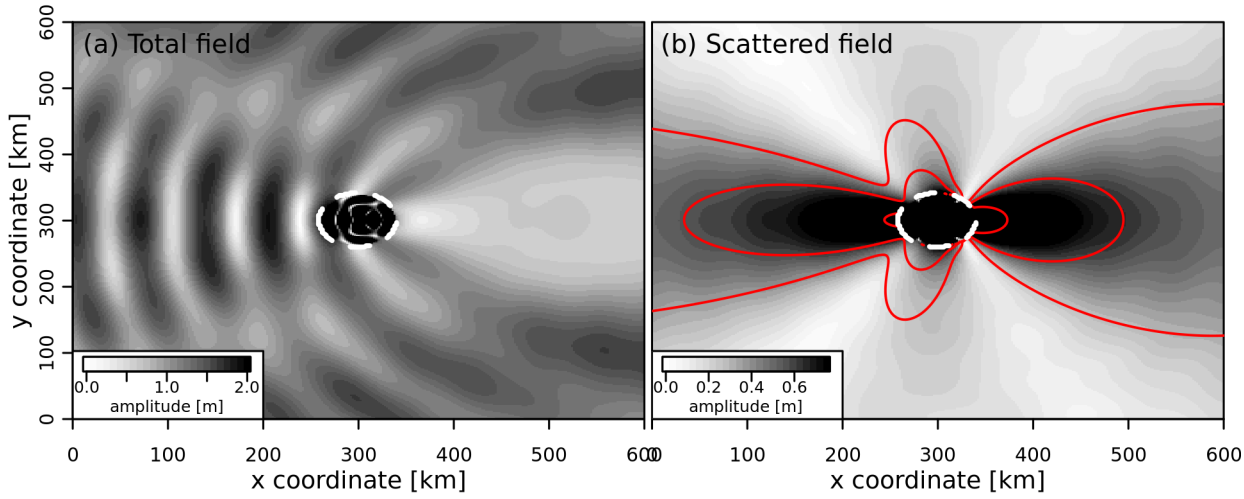


Figure 2: (a) Result of numerical experiment. (b) Scattered field alone with superposed analytical solution

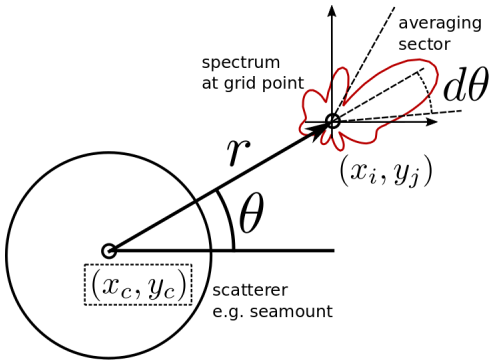


Figure 3: To definition of scattering amplitude from directional spectrum.

are fed into inverse model so that directional spectrum is estimated. The antenna is organized by concentric circles of radius $\lambda/2$, $\lambda/4$, $\lambda/8$ where $\lambda$ is a wavelength found from dispersion law of shallow-gravity waves. Each circle is discretized in 100 points that are projected to the nearest grid point, so actual number of points per circle might be smaller. The total field is a clear pattern of interference fringes following circularly spreading scattered from the seamount waves. At the same time due to large wavefront compare to wavelength there are diffractive maxima in the incident wavefield. It is clear that the wavefield is complex. It is unclear how much energy was transmitted into the scattered components and what its spatial structure. Here the scattered wavefield is reconstructed from spectrum as averaged sealevel emitted from the seamount in direction where spctrum is found (Figure 4a).

Figure 4a: Amplitude of Fourier coefficient of the total field of sea level. The antenna used at each grid point is shown as well. Period of the forced wave is 10 min.
Figure 4b: The scattered wave as Filtered out by application of the inverse method.
Figure 4c: The scattered wave as found by subtraction method.

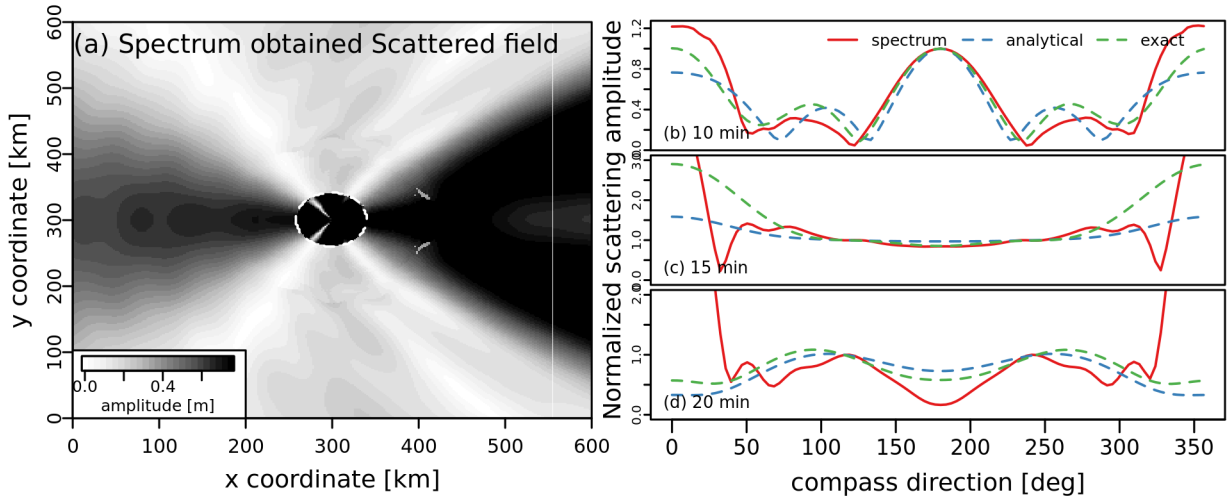


Figure 4: (a) Scattered field obtained from partial integration of spectrum. (b)-(d) Comparison of averaged scattering amplitude found by spectrum approach with exact scattered field and analytical solution in different regimes.

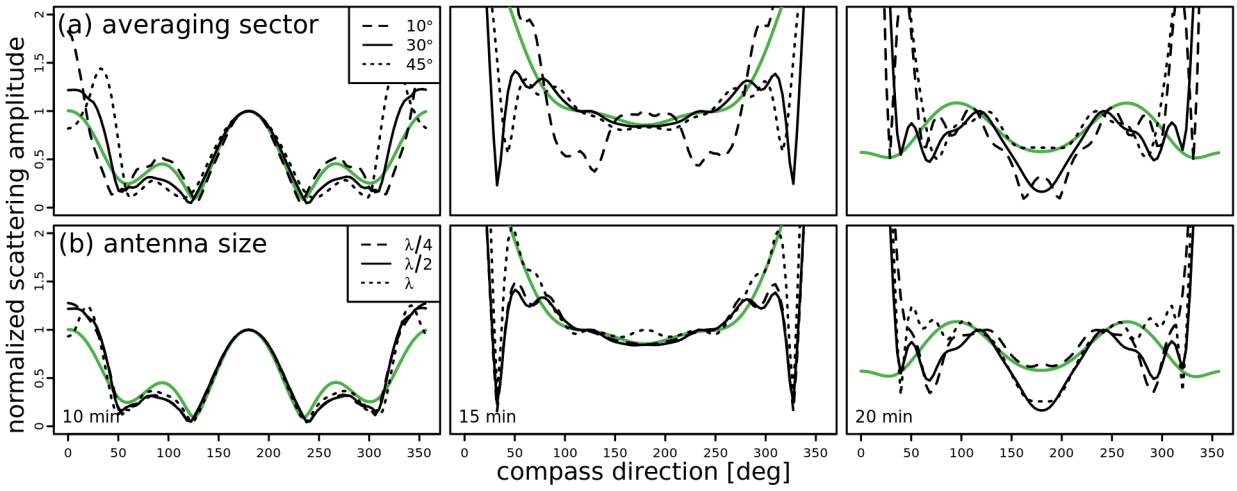


Figure 5: (a) Stability of scattering amplitude to change in averaging sector (row - (a)) and fitting window (row - (b)) for different wave periods. The green line shows exact scattered field.

Figure 5: Comparison of normalized scattering amplitude found by the inverse method and from subtraction method with analytical solution.

## 3.2 Results and discussion

## 3.3 Example: reflection of internal tide from step discontinuity

In the next problem an internal tide reflection from simplified topography is studied. The internal tide is given by the first baroclinic mode prescribed on the right side of channel with.
The MITgcm is employed where a nonrotating channel ends with discontinuity whose depth is changed. The channel depth is constant of 2000 m and ocean is uniformly stratified with Brunt-Vaisala frequency $N^2 = 1.5 \cdot 10^{-5}$. The horizontal resolution is 8 km. In vertical there are 25 equally discretized levels. Around the box sponges of 6 grid cells are set to absorb reflected waves.
On the right side a low-mode internal tide is prescribed with frequency of $M_2$ harmonic as perturbation in temperature profile and velocity field following respective mode-1 eigenfunction structure. Horizontally the basic field is perturbed over 450 km section to decrease diffractive effects. Additionally, the so-generated beam is let to freely propagate to get rid of edge effects and obtain spatially uniform field. The beam than impinges on a step topography where reflection and scattering into higher modes take place (Figure 6).
The model calculated fields are saved over two periods, harmonically analyzed. From temperature field one can obtain baroclinic pressure anomaly (Kelly et al. (2010)). This then are fit to eigenmode structure functions. So per each dynamical field quantity a complex amplitude is found. These are further used in spectrum estimate. The antenna for analysis is built in the same way as in previous example.
In such problems one is usually interested in estimate of energy being reflected. The reflected wave is defined here as all easterly propagating waves, i.e. compass directions located in the first and fourth quadrant. The energy flux is than can be reconstructed for these directions and compared with subtraction method (Figure 6b).
Energy conservation
The bulk reflection coefficient on the other hand can be obtained as a ratio of total incident energy going through a cross section and total reflected energy traveling away. As additional check this can be compared with results of analytical solution (Chapman & Hendershott (1981)) (Figure 7).

### 3.3.1 Test description

### 3.3.2 Results and discussion

# References

Arbic, B. K., Wallcraft, A. J., & Metzger, E. J. (2010). Concurrent simulation of the eddying general circulation and tides in a global ocean model. *Ocean Modelling*, *32*(3-4), 175–187.

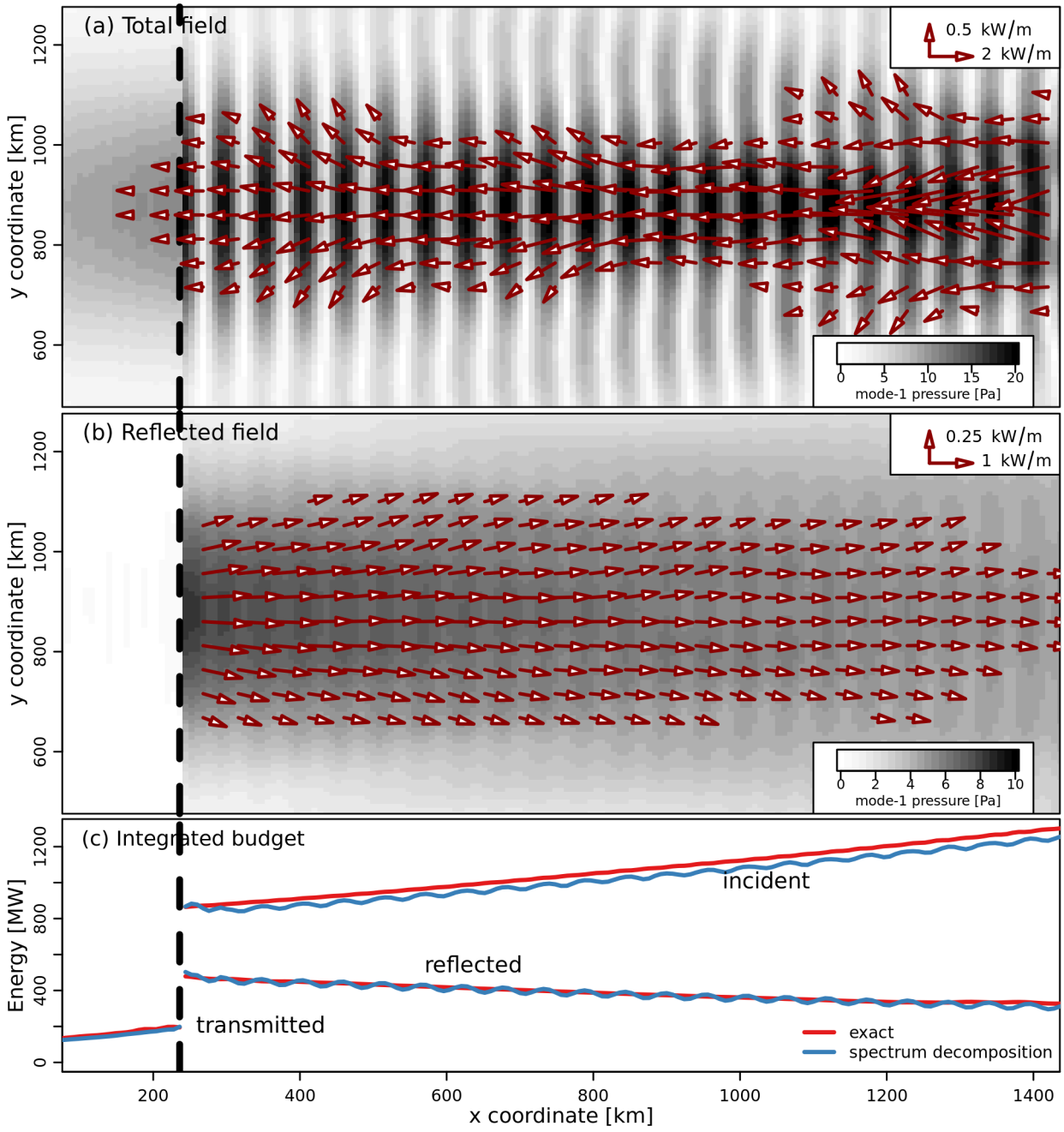


Figure 6: (a) Result of numerical experiment. (b) Reflected field found from directional spectrum. (c) Integrated energy transport.

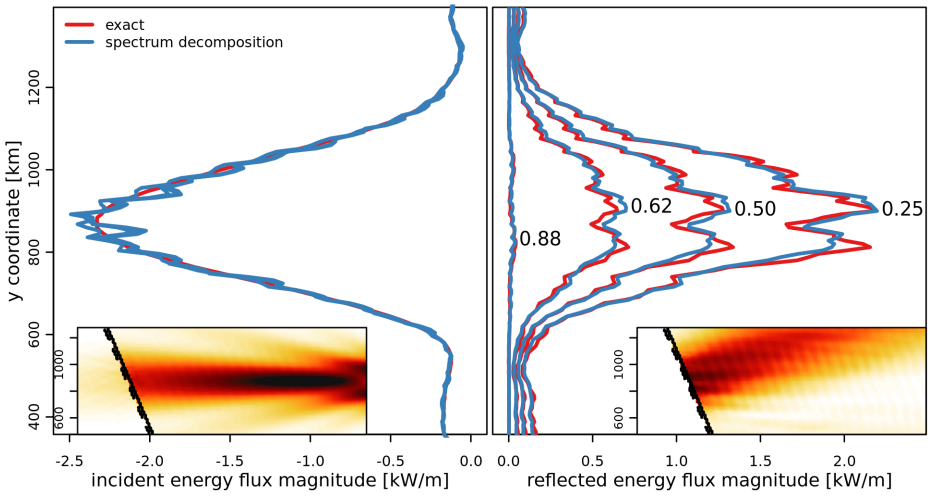


Figure 7: Oblique incidence experiment. (a) Distribution of incident field (a) and reflected (b). Insets show the corresponding spatial fields for depth ratio of 0.5.

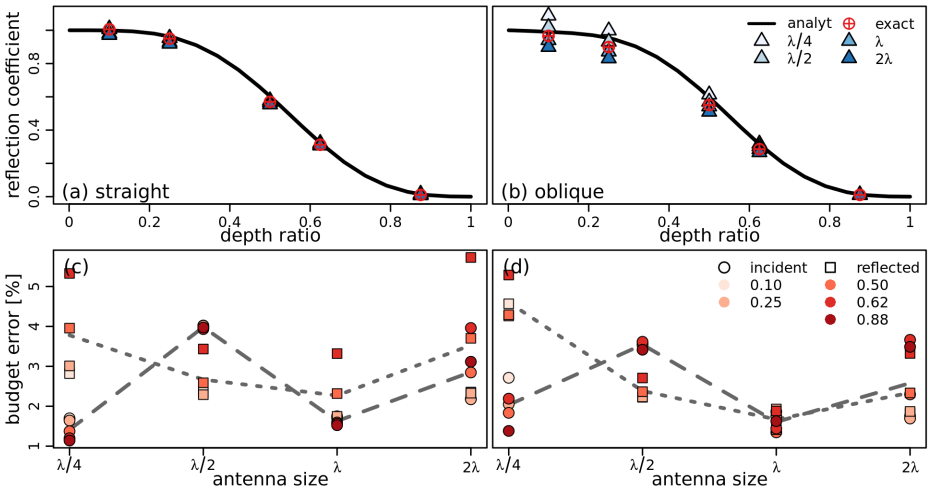


Figure 8: (a) and (b) Comparison of reflection coefficient between analytical theory, exact numerical solution and spectrum obtained estimate. Here results for different fitting window are given. (c) and (d) error in energy budget for incident (circles) and reflected (squares) and for different antenna sizes. Left column is for straight incidence experiments and right column for oblique incidence.

Barber, N. (1963). The directional resolving power of an array of wave detectors.

Bennett, A. F. (1992). *Inverse methods in physical oceanography*. Cambridge university press.

Benoit, M., Frigaard, P., & Schäffer, H. A. (1997). Analysing multidirectional wave spectra: a tentative classification of available methods. In *Proc. seminar on multidirectional waves and their interaction with structures* (pp. 131–158).

Chapman, D. C., & Hendershott, M. C. (1981). Scattering of internal waves obliquely incident upon a step change in bottom relief. *Deep Sea Research Part A. Oceanographic Research Papers*, *28*(11), 1323–1338.

Colton, D., & Kirsch, A. (1996). A simple method for solving inverse scattering problems in the resonance region. *Inverse problems*, *12*(4), 383.

Dickson, W., Herbers, T., & Thornton, E. (1995). Wave reflection from breakwater. *Journal of waterway, port, coastal, and ocean engineering*, *121*(5), 262–268.

Hansen, P. C., & OLeary, D. P. (1993). The use of the l-curve in the regularization of discrete ill-posed problems. *SIAM Journal on Scientific Computing*, *14*(6), 1487–1503.

Hashimoto, N., & Kobune, K. (1989). Directional spectrum estimation from a bayesian approach. In *Coastal engineering 1988* (pp. 62–76).

Hendry, R. (1977). Observations of the semidiurnal internal tide in the western north atlantic ocean. *Philosophical Transactions of the Royal Society of London A: Mathematical, Physical and Engineering Sciences*, *286*(1330), 1–24.

Herbers, T., & Guza, R. (1990). Estimation of directional wave spectra from multicomponent observations. *Journal of Physical Oceanography*, *20*(11), 1703–1724.

Kay, S. M., & Marple, S. L. (1981). Spectrum analysisa modern perspective. *Proceedings of the IEEE*, *69*(11), 1380–1419.

Kelly, S., Nash, J., & Kunze, E. (2010). Internal-tide energy over topography. *Journal of Geophysical Research: Oceans (1978–2012)*, *115*(C6).

Klymak, J. M., Simmons, H. L., Braznikov, D., Kelly, S., MacKinnon, J. A., Alford, M. H., ... Nash, J. D. (2016). Reflection of linear internal tides from realistic topography: The tasman continental slope. *Journal of Physical Oceanography*, *46*(11), 3321–3337.

Kowalik, Z., Knight, W., Logan, T., & Whitmore, P. (2005). Numerical modeling of the global tsunami: Indonesian tsunami of 26 december 2004. *Science of Tsunami Hazards*, *23*(1), 40–56.

Long, R. B. (1986). Inverse modeling in ocean wave studies. In *Wave dynamics and radio probing of the ocean surface* (pp. 571–593). Springer.

Long, R. B., & Hasselmann, K. (1979). A variational technique for extracting directional spectra from multi-component wave data. *Journal of Physical Oceanography*, *9*(2), 373–381.

Lozovatsky, I. D., Morozov, E. G., & Fernando, H. (2003). Spatial decay of energy density of tidal internal waves. *Journal of Geophysical Research: Oceans*, *108*(C6).

Mercier, M. J., Garnier, N. B., & Dauxois, T. (2008). Reflection and diffraction of internal waves analyzed with the hilbert transform. *Physics of Fluids*, *20*(8), 086601.

Munk, W., Worcester, P., & Wunsch, C. (2009). *Ocean acoustic tomography*. Cambridge University Press.

Munk, W. H., Miller, G., Snodgrass, F., & Barber, N. (1963). Directional recording of swell from distant storms. *Philosophical Transactions of the Royal Society of London A: Mathematical, Physical and Engineering Sciences*, *255*(1062), 505–584.

Pawka, S. (1983). Island shadows in wave directional spectra. *Journal of Geophysical Research: Oceans*, *88*(C4), 2579–2591.

Rafaely, B. (2004). Plane-wave decomposition of the sound field on a sphere by spherical convolution. *The Journal of the Acoustical Society of America*, *116*(4), 2149–2157.

Rhines, P. B. (1977). The dynamics of unsteady currents. *The sea*, *6*, 189–318.

Romano, A., Bellotti, G., & Di Risio, M. (2013). Wavenumber–frequency analysis of the landslide-generated tsunamis at a conical island. *Coastal Engineering*, *81*, 32–43.

Sacchi, M. D., & Ulrych, T. J. (1996). Estimation of the discrete fourier transform, a linear inversion approach. *Geophysics*, *61*(4), 1128–1136.

Sacchi, M. D., Ulrych, T. J., & Walker, C. J. (1998). Interpolation and extrapolation using a high-resolution discrete fourier transform. *IEEE Transactions on Signal Processing*, *46*(1), 31–38.

Simmons, H. L., Hallberg, R. W., & Arbic, B. K. (2004). Internal wave generation in a global baroclinic tide model. *Deep Sea Research Part II: Topical Studies in Oceanography*, *51*(25), 3043–3068.

Snieder, R., & Trampert, J. (1999). Inverse problems in geophysics. In *Wavefield inversion* (pp. 119–190). Springer.

Tang, L., Titov, V. V., Bernard, E. N., Wei, Y., Chamberlin, C. D., Newman, J. C., ... others (2012). Direct energy estimation of the 2011 japan tsunami using deep-ocean pressure measurements. *Journal of Geophysical Research: Oceans (1978–2012)*, *117*(C8).

Thomson, J., Elgar, S., & Herbers, T. (2005). Reflection and tunneling of ocean waves observed at a submarine canyon. *Geophysical research letters*, *32*(10).

Tikhonov, A. N., Goncharsky, A., Stepanov, V., & Yagola, A. G. (2013). *Numerical methods for the solution of ill-posed problems* (Vol. 328). Springer Science & Business Media.

Williams, E. G. (2001). Regularization methods for near-field acoustical holography. *The Journal of the Acoustical Society of America*, *110*(4), 1976–1988.

Zhao, Z., Alford, M. H., Girton, J. B., Rainville, L., & Simmons, H. L. (2016). Global observations of open-ocean mode-1 m2 internal tides. *Journal of Physical Oceanography*, *46*(6), 1657–1684.